



Article

# ATR–FTIR Spectral Analysis and Soluble Components of PM<sub>10</sub> And PM<sub>2.5</sub> Particulate Matter over the Urban Area of Palermo (Italy) during Normal Days and Saharan Events

Daniela Varrica <sup>1,\*</sup>, Elisa Tamburo <sup>1</sup>, Marcello Vultaggio <sup>2</sup> and Ida Di Carlo <sup>3</sup>

<sup>1</sup> Dipartimento Scienze della Terra e del Mare (DiSTeM), Via Archirafi 22, 90123 Palermo, Italy

<sup>2</sup> Risorse Ambiente Palermo (RAP), Piazzetta B. Cairoli, 90123 Palermo, Italy

<sup>3</sup> CNRS/INSU-Université d'Orléans—BRGM, UMR 7327, Institut des Sciences de la Terre d'Orléans, 1A rue de la Férollerie, 45071 Orléans, France

\* Correspondence: daniela.varrica@unipa.it; Tel.: +39-91-23861644

Received: 7 May 2019; Accepted: 26 June 2019; Published: 13 July 2019



**Abstract:** Several epidemiological studies have shown a close relationship between the mass of particulate matter (PM) and its effects on human health. This study reports the identification of inorganic and organic components by attenuated total reflectance-Fourier-transform infrared spectroscopy (ATR-FTIR) analysis in PM<sub>10</sub> and PM<sub>2.5</sub> filters collected from three air quality monitoring stations in the city of Palermo (Sicily, Italy) during non-Saharan dust events and Saharan events. It also provides information on the abundance and types of water-soluble species. ATR-FTIR analysis identified sulfate, ammonium, nitrate, and carbonate matter characterized by vibrational frequencies at 603, 615, 670, and 1100 cm<sup>-1</sup> (SO<sub>4</sub><sup>2-</sup>); at 1414 cm<sup>-1</sup> (NH<sub>4</sub><sup>+</sup>); at 825 and 1356 cm<sup>-1</sup> (NO<sub>3</sub><sup>-</sup>); and at 713, 730, and 877 cm<sup>-1</sup> (CO<sub>3</sub><sup>2-</sup>) in PM<sub>10</sub> and PM<sub>2.5</sub> filters. Moreover, aliphatic hydrocarbons were identified in the collected spectra. Stretching frequencies at 2950 cm<sup>-1</sup> were assigned to CH<sub>3</sub> aliphatic carbon stretching absorptions, while frequencies at 2924 and 2850 cm<sup>-1</sup> indicated CH<sub>2</sub> bonds. In filters collected during Saharan dust events, the analysis also showed the presence of absorbance peaks typical of clay minerals. The measurement of soluble components confirmed the presence of a geogenic component (marine spray and local rocks) and secondary particles ((NH<sub>4</sub>)<sub>2</sub>SO<sub>4</sub>, NH<sub>4</sub>NO<sub>3</sub>) in the PM filters. ATR-FTIR characterization of solid surfaces is a powerful analytical technique for identifying inorganic and organic compounds in samples of particulate matter.

**Keywords:** particulate matter; PM<sub>10</sub> and PM<sub>2.5</sub>; ATR-FTIR; ionic soluble components; saharan dust events; sirocco winds

## 1. Introduction

The urban air people breathe contains several solid and gaseous chemicals that have significant negative effects on public health [1–3]. Several epidemiological studies have shown a close relationship between air pollution and various respiratory tract diseases (allergies, asthma, lung emphysema), lung cancer, and cardiopulmonary mortality, which commonly affect urban populations [4–9]. The World Health Organization (WHO) [10] and the Directive of the European Parliament [11] established that daily values in Europe for concentrations of particulate matter with sizes of ≤10 and ≤2.5 μm (i.e., PM<sub>10</sub> and PM<sub>2.5</sub>) should not exceed 50 μg/m<sup>3</sup> and 25 μg/m<sup>3</sup>, respectively. Particulate matter with a size ≤10 μm is considered to be particularly detrimental to human health, but the nature of the PM is equally crucial as particle types have highly variable toxicity levels. Particulate matter comprises a range of particles such as mineral dust, metals, metalloids, sea salts, ammonium nitrate

and sulfate, organic compounds, and elemental carbon. The abundance of the various organic and inorganic components is temporally and spatially variable [12]. Some are directly emitted into the atmosphere by either natural or anthropogenic sources (primary particles), while others are the result of homogeneous or heterogeneous nucleation and condensation of gaseous precursors (secondary particles). The Mediterranean area is often affected by Saharan dust events, which increase PM<sub>10</sub> and PM<sub>2.5</sub> concentrations beyond European recommended values, mainly in southern Europe. Saharan dust is a mixture of mineral particles (quartz, calcite, dolomite, and clay minerals) and organic matter [13]. Some studies have suggested that Saharan dust has a significantly negative impact on air quality, visibility, and human health [14–16]. Several authors described increased asthma, rhinitis, cardiovascular disease, and mortality [17,18]. Other authors found no association between dust events and hospitalizations [19–23], increased mortality, or increased potential oxidative water-soluble fractions in PM<sub>10</sub> and PM<sub>2.5</sub> [24] compared to anthropogenic dust.

Water-soluble components (WSCs) are among the main components of total particulate matter [25,26], typically contributing about 50%–70% of the weight. WSCs are associated with degraded atmospheric visibility and adverse effects on human health [27–29]—they also contribute to the formation of acid rain, which promotes the faster decay of buildings. The main analytical technique used to determine water-soluble components is ion chromatography (IC). In recent years, Fourier-transform-infrared spectroscopy (FTIR) has become important in identifying aerosol composition and quantifying the mass of organic and inorganic compounds in particulate matter [30–33]. FTIR coupled with accessories like attenuated total reflectance (ATR) allows the analysis of a wide range of solid and liquid components [34].

In this study, we present data on the chemical composition of water-soluble components in PM<sub>10</sub> and PM<sub>2.5</sub> samples collected in an urban area of southern Italy. The city of Palermo, chosen for our case study, is affected by urban pollution and natural particulate matter from a range of sources. The principal sources in the study area are gasoline- and diesel-powered vehicles, an active commercial and tourist harbor, domestic heating, and a geogenic component that includes soil erosion, marine aerosol, and sporadic Saharan dust events. The aim of this paper is to identify the principal functional groups of inorganic and organic components in atmospheric aerosols by ATR-FTIR analysis. Moreover, we report the results of FTIR analysis carried out on samples of PM<sub>10</sub> and PM<sub>2.5</sub> filters taken during Saharan dust events that affected the Mediterranean area.

## 2. Materials and Methods

### 2.1. Site Details

Palermo is the largest urban area of Sicily, with about 680,000 inhabitants and a metropolitan area populated by more than 1 million people. The city is situated on the north-western coast of the island, bordered on the northeast by the Tyrrhenian Sea and surrounded by mountains (Monti di Palermo) reaching 500–1000 m above sea level (Figure 1).

The study area is entirely covered by sedimentary rocks (limestone, clay, marly-clay, and white or yellow quaternary biocalcarene). The climate of Palermo is typically Mediterranean, with hot summers and temperate winters. Among the stations studied, only Boccadifalco (BF) station records weather data representative of the entire agglomeration where the other stations of the present study (Giulio Cesare (GC) and Di Blasi (DB)) are located. Figure 2 shows the wind rose of the sampling period (November 2008–February 2009). From the monthly wind roses during the winter months, the prevailing wind direction is from the WNW and WSW sectors. In the same period, close to 5% wind direction from the S and SSE sectors (Sirocco winds) has been registered. During autumn and spring in the city, there are frequent warm winds coming from south-east (Sirocco winds) carrying dust raised from the Sahara Desert region throughout the Mediterranean basin. Over the sampling period, the weather monitoring station located in the peripheral area of Palermo (BF station) registered six periods of 1–2 days of Saharan dust intrusions.

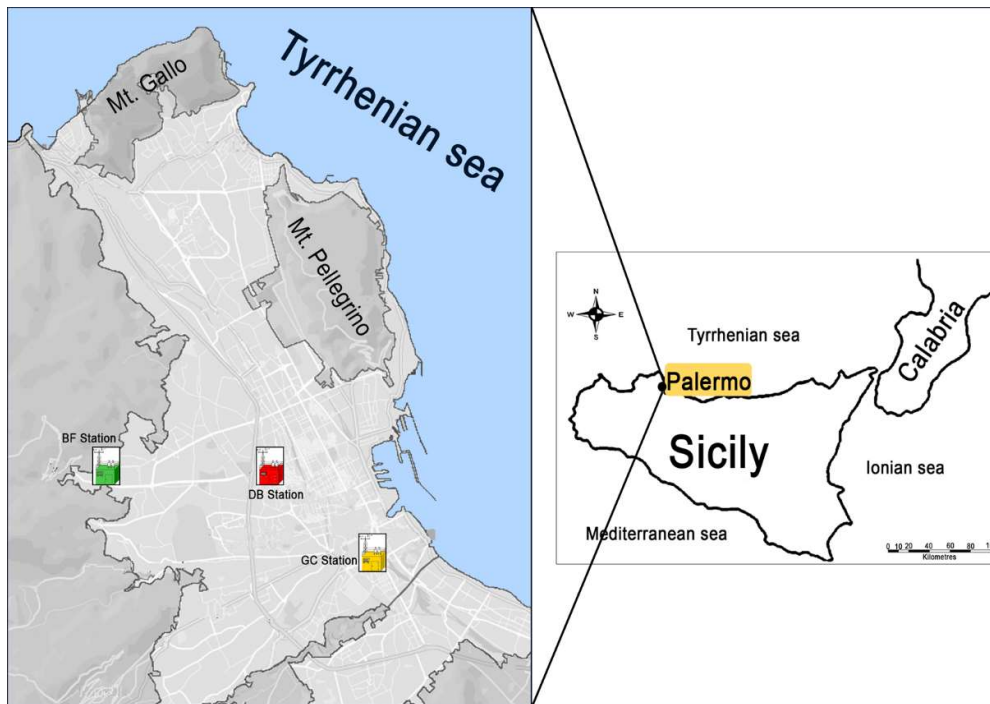


Figure 1. Location of study area with sampling sites. BF, Boccadifalco; DB, Di Blasi; GC, Giulio Cesare.

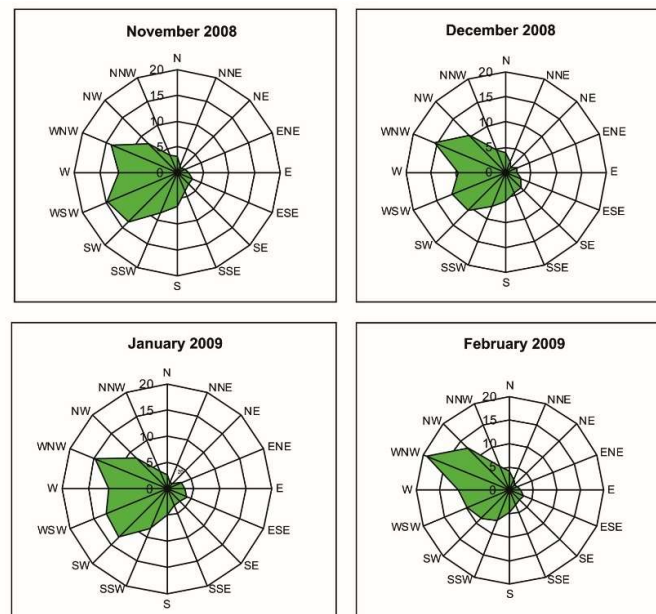


Figure 2. Prevailing winds at Palermo during the sampling period.

## 2.2. Sampling Sites

A total of 348 daily samples, 308  $PM_{10}$  and 40  $PM_{2.5}$ , were collected from November 2008 to February 2009. To meet the requirements of Directive 1999/30/EC (EU Commission, 1999),  $PM_{10}$  sampling was performed according to European Standard EN12341 (CEN, 1998), with a low-volume system equipped with a sampling inlet head (Zambelli Explorer Plus Controller 16) operating at a constant sampling rate ( $2.3 \text{ m}^3\text{h}^{-1}$ ). Particles were collected on standard 47 mm quartz filters (Advantec, grade QR100). The sampling time was 24 h, from midnight to midnight.  $PM_{2.5}$  sampling was performed according to European standard EN 14907 (CEN 2005). At Di Blasi (DB) station, simultaneous sampling

of PM<sub>10</sub> and PM<sub>2.5</sub> was carried out. PM<sub>10</sub> mass determination was performed by  $\beta$ -ray attenuation method, model Environment MP101M.C (CNR–Italy certified). The beta attenuation instrument is compliant with EN 12341 for PM<sub>10</sub> and is approved as federal equivalent method by US the Environmental Protection Agency for PM<sub>10</sub>. The detection is done every 2 hours (12 detections in 24 hours). Initial and final weighing of PM<sub>10</sub> and PM<sub>2.5</sub> filters were carried out in a temperature- and humidity-controlled room ( $T = 20 \pm 1$  °C,  $RH = 50 \pm 5\%$ ) after the filters had been conditioned for 48 h before and after sampling. Three air quality monitoring stations belonging to the municipal monitoring network (RAP-ex AMIA) were chosen for this study (Figure 1).

The Di Blasi (DB) station is located close to a crossroads with traffic lights at pedestrian crossings and is characterized by high traffic flow, consisting of cars, heavy-duty vehicles, and buses. Giulio Cesare (GC) station is situated in a large square in front of the railway station, exposed to heavy traffic composed of cars as well as urban and regional buses. The Boccadifalco (BF) station is a suburban background station, situated leeward of the sea breeze, without any direct influence of urban activities. It has lower traffic density than the other stations and was selected as a control site to monitor the hypothetical background level of pollution. Filters used for analysis were selected based on the simultaneity of daily sampling between the three monitoring stations. ATR-FTIR spectroscopy was used to analyze 13 PM<sub>10</sub> filters from the suburban background station (BF), 36 PM<sub>10</sub> filters from the urban station (GC), 40 PM<sub>2.5</sub> filters from the urban station (DB), and one composite sample of Saharan dust deposited in Palermo town. A total of 1 g of Saharan dust was taken near GC station using a plastic brush and tray and stored in plastic bags. The sample was initially sieved through a 63  $\mu$ m sieve to remove coarse components. Afterward, screening through a 20  $\mu$ m mesh sieve was necessary to obtain a finer fraction for FTIR analysis. The following were analyzed for water-soluble ions: 13 PM<sub>10</sub> filters from BF station, 30 PM<sub>10</sub> filters from GC station and 30 PM<sub>2.5</sub> filters from DB station.

### 2.3. Analytical Procedures

#### 2.3.1. FTIR Spectra

A Bruker Optics (Tensor 27) IR (Bruker Corporation, Billerica, MA, USA) spectrometer equipped with a deuterated triglyceride sulfate detector was operated with Opus software from Bruker to obtain the spectra of ambient air samples. An ATR accessory with a germanium crystal flat plate was coupled with the spectrometer for data acquisition. Aerosol sample spectra were obtained over wavelengths between 4000 and 400  $\text{cm}^{-1}$  (mid-infrared region) with 2  $\text{cm}^{-1}$  resolution by averaging 32 scans. Each aerosol sample was scanned by placing the quartz fiber filter sample-side down on the ATR crystal and applying the pressure tower. Each IR spectrum was corrected for optical effects with the ATR correction algorithm in Opus. A blank quartz fiber spectrum was obtained with each set of daily samples to account for any changes in the absorbance bands due to instrument drift. Between each sample spectrum acquisition, the ATR crystal was cleaned with ethanol, and an air background spectrum was obtained. The FTIR operation method is explained in Doyle [35] and Simonescu [36].

#### 2.3.2. Water-Soluble Ions

Water-soluble ions were extracted from filter samples with 20 mL ultra-pure Milli-Q (Merck Millipore, Burlington, MA, USA) water (18M $\Omega$  cm) and shaken for 24h. The extracts were filtered through a 0.45  $\mu$ m pore size polytetrafluoroethylene filter (Sartorius) and then stored in sterile 50 mL polypropylene centrifuge tubes. Each extract was analyzed the day after the extraction procedure for Ca<sup>2+</sup>, Mg<sup>2+</sup>, Na<sup>+</sup>, K<sup>+</sup>, Cl<sup>-</sup>, SO<sub>4</sub><sup>2-</sup>, and NO<sub>3</sub><sup>-</sup> ions by ion chromatography (Dionex 100), with precision better than  $\pm 5\%$ . Cations were measured using a Dionex IonPac CS12A (Thermo Fisher Scientific, Waltham, MA, USA) column with 20 mM methanesulfonic acid as the eluent. Anions were measured using a Dionex IonPac AS14 (Thermo Fisher Scientific, Waltham, MA, USA) with 3.5 mM Na<sub>2</sub>CO<sub>3</sub> and 1.0 mM NaHCO<sub>3</sub> as the eluent. The limit of detection was evaluated by solution extracts for three blank filters in 0.02–0.05 and 0.04–0.05 mg/L for cations and anions, respectively. NH<sub>4</sub><sup>+</sup> ions were

determined spectrophotometrically at  $\lambda = 420$  nm (Thermo Scientific Evolution 600) using Nessler's reagent (0.09 mol/L solution of potassium tetraiodomercurate (II) ( $K_2[HgI_4]$ ) in 2.5 mol/L potassium hydroxide). The ion chromatograph operation method is explained in Michalski [37].

### 3. Results and Discussion

#### 3.1. Mass Levels of $PM_{10}$ and $PM_{2.5}$

Table 1 shows the mass levels of  $PM_{10}$  at the urban and peripheral stations (GC, DB, and BF) and of  $PM_{2.5}$  at the urban DB station.

**Table 1.** Characteristics of  $PM_{10}$  and  $PM_{2.5}$  samples at the three monitoring stations during non-Saharan dust events and Saharan dust events. Mass values expressed in  $\mu\text{g}/\text{m}^3$ . # indicates measurements carried out simultaneously.

November 2008–February 2009				
	$PM_{10}$			$PM_{2.5}$
	BF station	GC station	DB station #	DB station #
N	95	108	105	40
Mean	16	39	42	29
Std.Dev.	7	11	11	6
Median	15	39	43	30
Min	8	16	13	13
Max	44	69	74	40
Q <sub>10</sub>	10	26	28	22
Q <sub>25</sub>	12	32	35	25
Q <sub>75</sub>	17	46	49	33
Q <sub>90</sub>	27	53	55	37
Saharan Dust Events				
N	7	7	8	4
Mean	130	158	133	78
Dev.St	89	81	59	28
Min	67	97	89	59
Max	261	276	220	120

The mean  $PM_{2.5}$  and  $PM_{10}$  concentrations fall within the range reported for European urban areas [38–40]. The highest mean  $PM_{10}$  value was observed at the urban DB station ( $42 \mu\text{g}/\text{m}^3$ ), one of the most heavily traffic-exposed sites in Palermo, followed by GC station ( $39 \mu\text{g}/\text{m}^3$ ) and BF station ( $16 \mu\text{g}/\text{m}^3$ ). The average  $PM_{2.5}$  value observed at DB station is  $29 \mu\text{g}/\text{m}^3$ . For the 112 days analyzed (November 2008–February 2009), Saharan dust events influenced mass levels in the Palermo atmosphere on about 6% of the days. During these events, concentrations of  $130$ – $158 \mu\text{g}/\text{m}^3$  and  $78 \mu\text{g}/\text{m}^3$  were measured for  $PM_{10}$  and  $PM_{2.5}$ , respectively. In Palermo in February 2009,  $PM_{2.5}$  reached a daily concentration of  $120 \mu\text{g}/\text{m}^3$  and  $PM_{10}$  reached values between 220 and  $276 \mu\text{g}/\text{m}^3$  following a high-intensity Saharan dust event. The value of  $PM_{2.5}$  is comparable to that found by Remoundaki et al. [41] in Athens in February 2009 ( $100 \mu\text{g}/\text{m}^3$ ). During other, less-intense Saharan dust events,  $PM_{2.5}$  concentrations (average  $62 \mu\text{g}/\text{m}^3$ ) increased by 50% and  $PM_{10}$  (average  $86$ – $119 \mu\text{g}/\text{m}^3$ ) by 65–80%. The values reported are higher than those published in previous studies concerning southern Italy (Rome:  $PM_{2.5}$ ,  $25.6 \mu\text{g}/\text{m}^3$ ;  $PM_{10}$ ,  $47.2 \mu\text{g}/\text{m}^3$  [16]; Salento:  $PM_{2.5}$ ,  $36.6 \mu\text{g}/\text{m}^3$ ;  $PM_{10}$ ,  $137 \mu\text{g}/\text{m}^3$  [24]; Bari:  $PM_{2.5}$ ,  $31$ – $49 \mu\text{g}/\text{m}^3$ ;  $PM_{10}$ ,  $50$ – $71 \mu\text{g}/\text{m}^3$  [42]), but the higher percentages during Saharan dust events are comparable [24,43–45]. In general, the contribution of particulate matter is evidenced in coarse rather than fine fractions [41]. The influence of Saharan dust on the Mediterranean basin has been estimated to be about 10–20% per year, thus many European countries have exceeded the PM limits recommended by the European Directive. The  $PM_{2.5}/PM_{10}$  ratio has been widely used in

environmental studies as an indicator of the contribution from stationary vs. mobile source emissions to the environment.

The average  $PM_{2.5}/PM_{10}$  ratio measured at DB station is 0.70. This value is typical of urban environments with high traffic density [26,40,46–49]. During Saharan events, the  $PM_{2.5}/PM_{10}$  ratio was only 0.58, indicating a greater natural contribution of coarse than fine particles.

### 3.2. Spectral Analysis

The ATR spectra of  $PM_{10}$  and  $PM_{2.5}$  are shown in Figure 3a–c. The spectra identify different inorganic and organic molecules (Table 2).

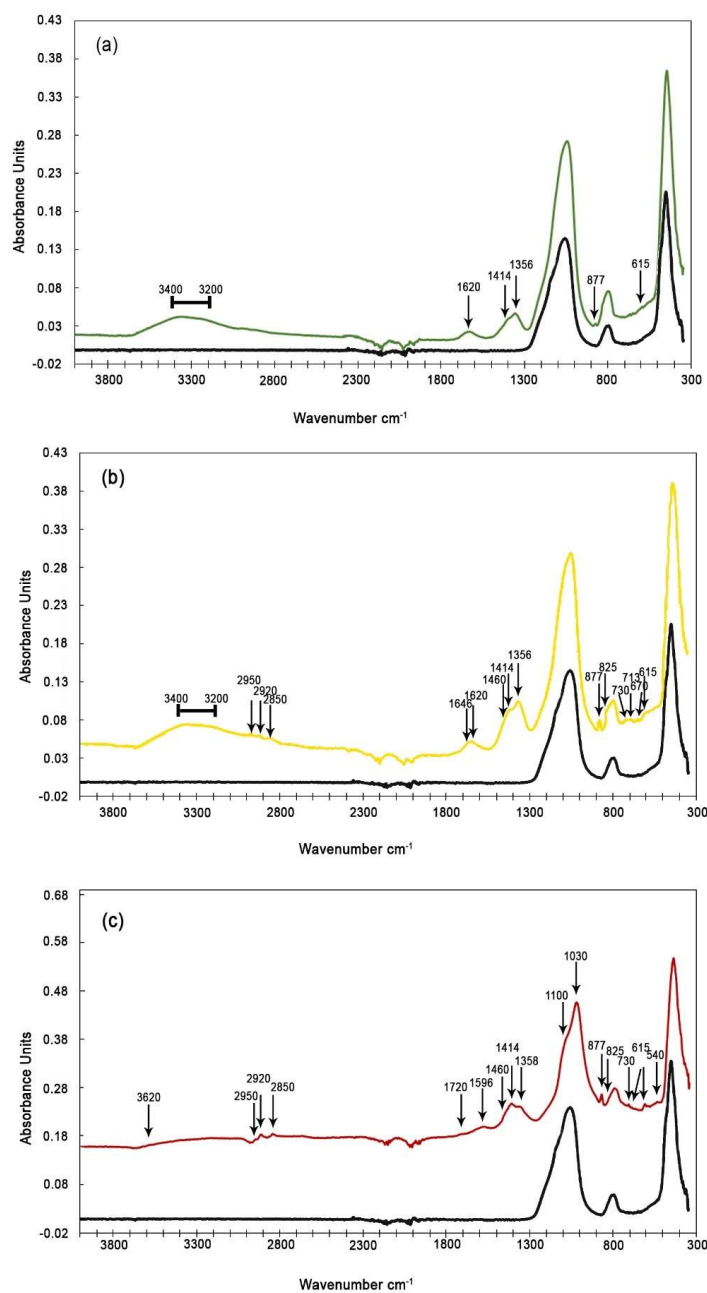


**Figure 3.** FTIR spectra of (a) suburban  $PM_{10}$  filter (BF station); (b) urban  $PM_{10}$  filter (GC station); and (c) urban  $PM_{2.5}$  filter (DB station). For each spectrum, we also report the spectrum of a blank quartz filter (black line) for comparison.

Some peaks have no well-defined forms, and the presence of a shoulder indicates that there are overlapping peaks due to several different types of molecules absorbing IR radiation within the same range. From comparing the spectra, it is observed that the samples are dominated by inorganic components common to all stations.

In PM<sub>10</sub> and PM<sub>2.5</sub> filters, we observed vibrational frequencies typical for sulfate, ammonium, nitrate, and carbonate ions (603, 615, 670, and 1100 cm<sup>-1</sup> (SO<sub>4</sub><sup>2-</sup>); 1414 cm<sup>-1</sup> (NH<sub>4</sub><sup>+</sup>); 825 and, 1356 cm<sup>-1</sup> (NO<sub>3</sub><sup>-</sup>); and 713, 730, and 877 cm<sup>-1</sup> (CO<sub>3</sub><sup>2-</sup>). The presence of (NH<sub>4</sub>)<sub>2</sub>SO<sub>4</sub> and NH<sub>4</sub>NO<sub>3</sub> compounds is supported by spectra shown in Figure 3b,c revealing absorption frequencies at 825 and 1356 cm<sup>-1</sup> (group NO<sub>3</sub><sup>-</sup>), at 615 and 1100 cm<sup>-1</sup> (group SO<sub>4</sub><sup>2-</sup>), and at 1414 cm<sup>-1</sup> (NH<sub>4</sub><sup>+</sup> ion) [30,50]. The inferred 1100 cm<sup>-1</sup> peak is a shoulder of the peak observed at 1060 cm<sup>-1</sup>. The 1100 cm<sup>-1</sup> peak is assigned to the ν<sub>3</sub> asymmetrical stretching vibration of sulfate ion [51,52].

In all spectra (for coarse and fine particles), absorption frequencies at 1620 cm<sup>-1</sup> and in the range of 3240–3400 cm<sup>-1</sup> have been detected that can be attributed to O–H stretching, indicating crystalline water in gypsum [34,53].

The presence of CaSO<sub>4</sub> × 2H<sub>2</sub>O is more evident in coarse than fine particles. The common presence of CaSO<sub>4</sub> × 2H<sub>2</sub>O signals supports the widely accepted hypothesis that the sulfation process is important in urban environments [54]. Varrica et al. [55] observed CaSO<sub>4</sub> × 2H<sub>2</sub>O crust on CaCO<sub>3</sub> particles by scanning electron microscopy (SEM) of samples also collected in Palermo. In samples of “black crust” formed on historical buildings in Palermo, Montana et al. [56] determined δ<sup>34</sup>S values ranging from –0.5 to +5.0‰ (vs. Vienna Cañon Diablo Troilite (VCDT) scale), which suggests that most of the sulfur was derived from fossil fuel combustion. Moreover, Cesari et al. [43] observed that during Saharan dust events, the dominant form of sulfate is calcium sulfate rather than (NH<sub>4</sub>)<sub>2</sub>SO<sub>4</sub>. The absorption peaks at 713, 730, and 877 cm<sup>-1</sup> are typical for the CO<sub>3</sub> group [53,57,58], and the FTIR analysis of pure crystalline calcite and dolomite confirms that these peaks are related to CaCO<sub>3</sub>. The peaks of halite between 1000 and 1200 cm<sup>-1</sup> are not clearly visible due to the absorption linked with the quartz filter. In the GC and BF samples, there is also a peak at 1620 cm<sup>-1</sup> that can be attributed to one of the peaks of halite; at 1414 cm<sup>-1</sup> the peak of halite is not visible as it is very small and overlaps with the ammonium ion peak.

**Table 2.** Typical peaks of inorganic and organic molecules identified in filter samples during non-Saharan events and Saharan dust events.

Species	Frequency (cm <sup>-1</sup> ) in This Study	Frequency (cm <sup>-1</sup> ) from Literature	References
<b>Non-Saharan Events</b>			
SO <sub>4</sub> <sup>2-</sup>	603; 615; 670; 1100	608; 615; 670; 1100	[30,35,36,51–53]
CO <sub>3</sub> <sup>2-</sup>	713; 730; 877	713; 730; 873; 877	[53,57,58]
NO <sub>3</sub> <sup>-</sup>	825; 1356	825; 1318–1410; 1350	[30,58]
NH <sub>4</sub> <sup>+</sup>	1414	1414	[50]
C=C	1510–1596	1463–1511–1596	[59,61]
C-H	1460; 2850; 2920; 2950	2850–2920; 2800–3000	[30,31,34,58–60]
Water (OH)	1620; 3200–3400; 3620	1620; 3200–3400; 3620	[34,53,62]
Al-O-Si	540	540	[57,58]
Si-O	1030	1030	[30,62]
C=O	1720	1720; 1722	[34,58]
<b>Saharan Dust Events</b>			
O-Si-O	423; 463; 520	426; 468; 525	[63]
SO <sub>4</sub> <sup>2-</sup>	603; 615; 670; 1110	608; 615; 670; 1100	[30,60]
CO <sub>3</sub> <sup>2-</sup>	713; 730; 780; 877; 1433	713; 730; 873; 877	[58,62]
Al-O-Si	750	750	[63,64]
Al-Al-OH	912	910	[62,65]
NO <sub>3</sub> <sup>-</sup>	825; 1356	825; 1318–1410; 1350	[30,32,58]
NH <sub>4</sub> <sup>+</sup>	1414	1414	[50]
C=C	1510–1596	1463–1511–1596	[59,61]
C-H	1460; 2800–3000	1460; 2850–2920; 2800–3000	[30,31,34,58,59]
Water (OH)	688; 1620; 1685; 3260–3400; 3620; 3669; 3695	688; 1620; 3200–3400; 3620, 3669; 3695	[34,62,63,66]
Si-O	1010; 1032	1010; 1030; 1031	[30,62,67]

Organic compounds are identified in the coarse and fine particle fractions of the urban stations but are absent from the filters collected at the suburban station. The aliphatic hydrocarbons ( $2850$ ,  $2920$ , and  $2950\text{ cm}^{-1}$ ) were clearly identified in the collected spectra (Figure 3b,c) [30,31,34,59–61]. The stretching frequency at  $2950\text{ cm}^{-1}$  is assigned to  $\text{CH}_3$  aliphatic carbon stretching absorption, while the frequencies at  $2924$  and  $2850\text{ cm}^{-1}$  are due to  $\text{CH}_2$  bonds. An absorption peak at  $1460\text{ cm}^{-1}$  comprises contributions from bending of  $\text{CH}_3$  and  $\text{CH}_2$  aliphatic carbon bonds [30,59]. Vibration around  $1460\text{ cm}^{-1}$  is a shoulder of the peak at  $1414\text{ cm}^{-1}$ . The spectra for  $\text{PM}_{2.5}$  filters also show an absorbance peak at  $1596\text{ cm}^{-1}$ , identified as a  $\text{C}=\text{C}$  group [59,61]. The identification of other peaks for  $\text{C}=\text{C}$  aromatic group ( $1463$ – $1511$ – $1596\text{ cm}^{-1}$ ) is complicated by overlapping peaks due to several different types of molecules that absorb IR radiation within the same range.

### 3.3. Spectral Analysis Of Samples Collected During Saharan Dust Episodes

The particulate matter collected during Saharan dust events show peaks belonging to a group of clay minerals, which were not detected during non-Saharan events. Figure 4 shows the ATR spectra of the urban area (GC)  $\text{PM}_{10}$  filter, the urban area (DB)  $\text{PM}_{2.5}$  filter, and the Saharan dust.

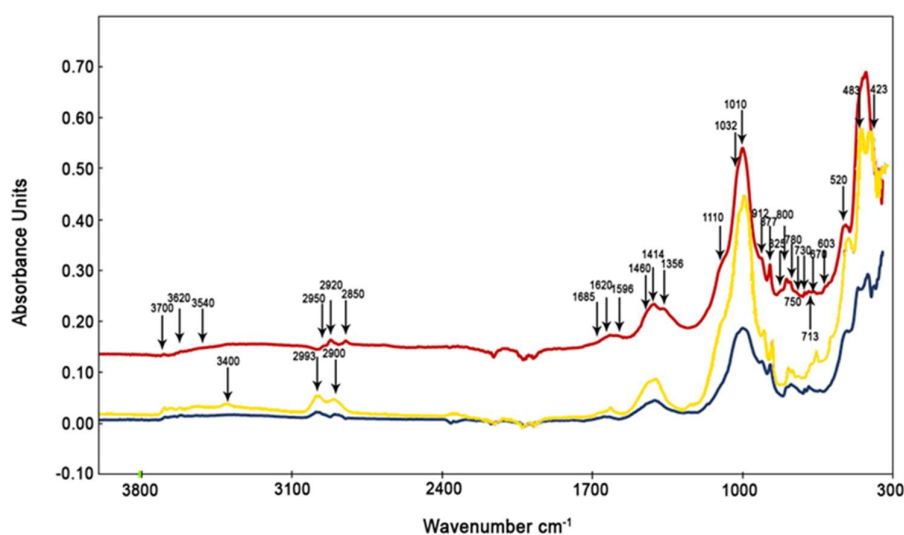


**Figure 4.** FTIR spectra of urban  $\text{PM}_{10}$  (GC, yellow line) and  $\text{PM}_{2.5}$  (DB, red line) filters. Blue line is FTIR spectrum of Saharan dust deposited in Palermo.

Peaks at wavenumbers of  $423$ ,  $463$ , and  $520\text{ cm}^{-1}$  are associated with the  $\text{O}-\text{Si}-\text{O}$  bending of palygorskite and illite ( $426$ ,  $468$ , and  $525\text{ cm}^{-1}$ ) [63]. The peak at  $750\text{ cm}^{-1}$  identifies the inner layer vibration of  $\text{Al}-\text{O}-\text{Si}$  groups in illite [63,64]. Previous studies assigned the peak at  $912\text{ cm}^{-1}$  to the deformation of  $\text{Al}-\text{Al}-\text{OH}$  groups in the dioctahedral layer of palygorskite [62,65]. The identification of kaolinite is characterized by the presence of peaks at  $1010$ ,  $1032$ , and  $1114\text{ cm}^{-1}$ , representing the  $\text{Si}-\text{O}$  stretching group [67]. Peaks at  $1032$  and  $1114\text{ cm}^{-1}$  are not distinct because they simultaneously characterize various molecules that vibrate in the same IR intervals, creating peak overlaps.

Peaks at  $3260$ ,  $3400$ ,  $3620$ ,  $3669$ , and  $3695\text{ cm}^{-1}$  are all linked to the vibration of  $-\text{OH}$  groups belonging to different clay minerals. Peaks at  $3260$  and  $3400\text{ cm}^{-1}$  are reported to relate to water stretching in palygorskite [63,65]. The  $\text{OH}$  groups located between tetrahedral and octahedral sheets are characterized by absorption near  $3620\text{ cm}^{-1}$  in all clay minerals. They reside at the octahedral surface of the layers, forming weak hydrogen bonds with the oxygens of the  $\text{Si}-\text{O}-\text{Si}$  bonds on the lower surface of the next layer. A strong band at  $3695\text{ cm}^{-1}$  relates to the in-phase symmetric stretching vibration. Weak absorptions at  $3669\text{ cm}^{-1}$  are assigned to out-of-plane stretching vibrations [68,69]. In these samples, we found the same organic components as observed in the samples taken during non-Saharan events.



### 3.4. Water-Soluble Ions

Table 3 shows the mean concentrations of soluble components of PM<sub>10</sub> and PM<sub>2.5</sub> filters. Inorganic ions represent about 50%–70% of the total mass of PM<sub>10</sub> and PM<sub>2.5</sub>.

**Table 3.** Soluble ion concentrations. Data expressed in  $\mu\text{g}/\text{m}^3$ . nss, non-sea salt;  $\Sigma\text{TP}$ , total mass of ions; TPM, total particulate matter ( $\mu\text{g}/\text{m}^3$ ).

	PM <sub>10</sub>		PM <sub>2.5</sub>
	BF station	GC station	DB station
F <sup>-</sup>	0.15	0.15	0.17
Cl <sup>-</sup>	1.19	1.70	0.64
NO <sub>3</sub> <sup>-</sup>	2.30	4.13	2.91
SO <sub>4</sub> <sup>2-</sup>	2.69	2.26	2.49
Na <sup>+</sup>	1.14	1.47	0.74
K <sup>+</sup>	0.23	0.27	0.23
Mg <sup>2+</sup>	0.20	0.24	0.09
Ca <sup>2+</sup>	0.78	1.60	1.33
NH <sub>4</sub> <sup>+</sup>	0.96	1.32	1.52
nssSO <sub>4</sub> <sup>2-</sup>	2.44	2.05	2.10
$\Sigma\text{TM}$	9.64	13.1	10.1
TPM	19.5	37.0	29.3

About 60% and 70% of total ions analyzed in PM<sub>10</sub> and PM<sub>2.5</sub> filters, respectively, are made up of NH<sub>4</sub><sup>+</sup>, NO<sub>3</sub><sup>-</sup>, and SO<sub>4</sub><sup>2-</sup>. For urban stations (PM<sub>10</sub> and PM<sub>2.5</sub>) the ammonium and calcium ions (expressed in  $\text{neq}/\text{m}^3$ ) are the most abundant cations. Magnesium and potassium are less abundant, contributing only about 1% to the total content of particulate matter. If the soluble calcium is derived from the alteration of carbonate rocks, a geogenic contribution of 10–14% of the total mass of the PM<sub>10</sub> fraction from urban and suburban stations is estimated. In the fine PM<sub>2.5</sub> fraction, a geogenic contribution is estimated to account for 9% of the total mass at the urban station.

NO<sub>3</sub><sup>-</sup> and SO<sub>4</sub><sup>2-</sup> anions have the highest concentration at all stations. In this study, the contribution of marine sulfate was calculated to have been around 6–10% in PM<sub>10</sub> and 3% in PM<sub>2.5</sub> fractions. The main source of SO<sub>4</sub><sup>2-</sup> in the atmosphere is from gas-to-particle conversion of SO<sub>2</sub>. NO<sub>3</sub><sup>-</sup> ions derive from the reaction of hydroxyl radicals, formed by photolysis of ozone molecules, with NO<sub>x</sub> emitted by fossil fuel combustion. High concentrations of ammonium, sulfate, and nitrate ions demonstrate their involvement in secondary particulate formation. A significant correlation between NH<sub>4</sub><sup>+</sup> and (nssSO<sub>4</sub><sup>2-</sup> + NO<sub>3</sub><sup>-</sup>) has been found ( $r = 0.90$ ,  $p < 0.05$ ; Figure 5), confirming the formation of ammonium sulfate and nitrate following neutralization of aerosol through heterogeneous atmospheric chemical reactions [47,70–72].

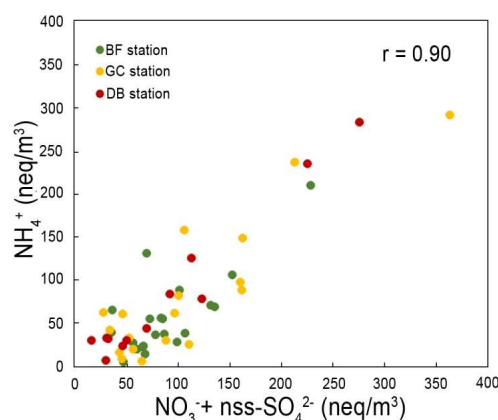


**Figure 5.** Plot of NO<sub>3</sub><sup>-</sup>+nss-SO<sub>4</sub><sup>2-</sup> vs NH<sub>4</sub><sup>+</sup> ion concentrations. Data expressed in  $\text{neq}/\text{m}^3$ .

These sequences of reactions are strongly influenced by ambient temperature, relative humidity conditions, incidence of solar radiation, and above all the concentration of primary gases [73]. The equivalent ratio of  $\text{NH}_4^+/\text{nss-SO}_4^{2-}$  in urban  $\text{PM}_{10}$  and  $\text{PM}_{2.5}$  is more than 1.5, characterizing the ambient atmosphere as ammonium-rich [74]. Nevertheless, as Figure 5 shows, the concentration of ammonium ions is insufficient to completely neutralize  $\text{H}_2\text{SO}_4$  and  $\text{HNO}_3$ . Total neutralization of the acid species is linked to the presence of carbonate rocks, abundant in the study area. The highest chlorine and sodium contents found in coarse samples (GC and BF) range between 1.70 and 1.19  $\mu\text{g}/\text{m}^3$  and 1.14 and 1.45  $\mu\text{g}/\text{m}^3$ , respectively. The main source of  $\text{Cl}^-$  and  $\text{Na}^+$  in the study area is marine spray, accounting for 11–15% of the total mass in the  $\text{PM}_{10}$  fraction from urban and suburban stations. For fine  $\text{PM}_{2.5}$  fraction, sea salt contribution is estimated to account for 9% of the total mass at DB station. The average Na/Cl equivalent ratio measured in the  $\text{PM}_{10}$  and  $\text{PM}_{2.5}$  filters ranges between 1.4 and 1.8. These values are higher than those of seawater (0.85) and halite (1.0), suggesting a loss of chlorine ions due to chemical reactions that involve NaCl and  $\text{HNO}_3$  or  $\text{H}_2\text{SO}_4$ , bringing the formation of  $\text{NaNO}_3$  or  $\text{Na}_2\text{SO}_4$  and gaseous HCl [66]. Similarly, a deficit of ammonium with respect to the collective concentration of  $\text{SO}_4^{2-}$  and  $\text{NO}_3^-$  ( $\text{neq}/\text{m}^3$ ) suggests that a proportion of these ions is lost via formation of  $\text{NH}_4\text{Cl}$  or HCl and  $\text{NH}_3$  [47,51].

#### 4. Conclusions

The main objective of this study was to verify the potential of ATR-FTIR to identify organic and inorganic groups present in  $\text{PM}_{10}$  and  $\text{PM}_{2.5}$ . The use of ATR-FTIR led to the identification of absorption bands characteristic of sulfate, ammonium, nitrate, and carbonate by vibrational frequencies at 603, 615, 670, and 1100  $\text{cm}^{-1}$  for  $\text{SO}_4^{2-}$ , at 1414  $\text{cm}^{-1}$  for  $\text{NH}_4^+$ , at 825 and 1356  $\text{cm}^{-1}$  for  $\text{NO}_3^-$ , and at 713, 730, and 877  $\text{cm}^{-1}$  for  $\text{CO}_3^{2-}$  common to all filter types ( $\text{PM}_{10}$  and  $\text{PM}_{2.5}$ ). Vibration frequencies at 1620  $\text{cm}^{-1}$  and in the range of 3240–3400  $\text{cm}^{-1}$  indicate O–H stretching of crystalline water in gypsum. The presence of gypsum in the particulate matter of Palermo confirms the hypothesis that sulfation processes play an important role in urban areas. Moreover, in urban spectra, several organic compounds were identified, while aliphatic compounds were not detected at the suburban station. The ATR-FTIR analysis of filters taken during Saharan dust events shows the presence of absorbance peaks typical for clay minerals. The minerals found were palygorskite, illite, and kaolinite, which are typical for Saharan desert environments.

The water-soluble components represent about 50%–70% of the total mass of  $\text{PM}_{10}$  and  $\text{PM}_{2.5}$ . Nitrate and sulfate ions had the highest concentrations at all stations, confirming their involvement in secondary particulate formation. The results show that ammonium ions are not able to neutralize most of the nitric and sulfuric acids present in aerosols. The main geogenic sources in the study area are marine spray and local rocks.

The data of this study shows that ATR-FTIR, used here as a qualitative approach, is a powerful analytical technique for the identification of inorganic and organic compounds in  $\text{PM}_{10}$  and  $\text{PM}_{2.5}$  filters. Moreover, the simplicity of the substrate preparation, the excellent reproducibility of the results, the non-destruction of the sample, and above all the fast identification of components of particulate matter confirm the opportunity to use this analytical technique for qualitative analysis, and to characterize variations in the chemical composition of aerosol particles during intense pollution episodes.

**Author Contributions:** Conceptualization, D.V. and I.D.C.; Data curation, D.V., E.T. and I.D.C.; Formal analysis, D.V., E.T. and I.D.C.; Funding acquisition, D.V.; Methodology, M.V.; Writing—original draft, D.V., E.T. and I.D.C.

**Acknowledgments:** This work was supported by Miur (funds FFR2018, D. Varrica). We would like to thank Risorse Ambiente Palermo (RAP, ex AMIA) of Palermo (Italy) (<http://www.rapspa.it/site/>) for providing the filter samples.

**Conflicts of Interest:** The authors declare no conflict of interest.

## References

1. Schell, L.M.; Denham, M. Environmental Pollution in Urban Environments and Human Biology. *Annu. Rev. Anthropol.* **2003**, *32*, 111–134. [[CrossRef](#)]
2. Sancini, A.; Tomei, F.; Tomei, G.; Caciari, T.; Di Giorgio, V.; André, J.C.; Palermo, P.; Andreozzi, G.; Nardone, N.; Schifano, M.P.; et al. Urban pollution. *G. Ital. Med. Lav. Ergon.* **2012**, *34*, 187–196. [[PubMed](#)]
3. Kelly, F.J.; Fussell, J.C. Air pollution and public health: Emerging hazards and improved understanding of risk. *Environ. Geochem. Health* **2015**, *37*, 631–649. [[CrossRef](#)] [[PubMed](#)]
4. Miller, K.A.; Siscovick, D.S.; Sheppard, K.; Sullivan, J.H.; Anderson, G.L.; Kaufman, J.D. Long-term exposure to constituents of fine particulate air pollution and incidence of cardiovascular events in women. *N. Engl. J. Med.* **2007**, *356*, 447–458. [[CrossRef](#)] [[PubMed](#)]
5. Pope, C.A.; Burnett, R.T.; Thun, M.J.; Calle, E.E.; Krewsky, D.; Ito, K.; Thurston, G.D. Lung cancer, cardiopulmonary mortality, and long-term exposure to fine particulate air pollution. *JAMA* **2002**, *287*, 1132–1141. [[CrossRef](#)] [[PubMed](#)]
6. Pope, C.A.; Ezzati, M.; Dockery, D.W. Fine-Particulate Air Pollution and Life Expectancy in the United States. *N. Engl. J. Med.* **2009**, *360*, 376–386. [[CrossRef](#)] [[PubMed](#)]
7. Van Donkelaar, A.; Martin, R.V.; Michael Brauer, M.; Boys, B.L. Use of Satellite Observations for Long-Term Exposure Assessment of Global Concentrations of Fine Particulate Matter. *Environ. Health Perspect.* **2015**, *123*, 135–143. [[CrossRef](#)]
8. Lipfert, F.W. Long-term associations of morbidity with air pollution: A catalog and synthesis. *J. Air Waste Manag. Assoc.* **2018**, *68*, 12–28. [[CrossRef](#)]
9. Liu, M.; Xue, X.; Zhou, B.; Zhang, Y.; Baijun, S.; Chen, J.; Li, X. Population susceptibility differences and effects of air pollution on cardiovascular mortality: Epidemiological evidence from a time-series study. *Environ. Sci. Pollut. Res.* **2019**, *26*, 15943–15952. [[CrossRef](#)]
10. World Health Organization (WHO). *Air Quality Guidelines for Europe*, 2nd ed.; WHO Regional Publications, 91; World Health Organization, Regional Office for Europe: Copenhagen, Denmark, 2000.
11. EU-Commission. *Directive 2008/50/EC of the European Parliament and of the Council of 21 May 2008 on Ambient Air Quality and Cleaner Air for Europe Official Journal of the European Union L152/3 (11/06/2008)*, 6–15; EU-Commission: Brussels, Belgium, 2008.
12. Squizzato, S.; Cazzaro, M.; Innocente, E.; Visin, F.; Hopke, P.K.; Rampazzo, G. Urban air quality in a mid-size city—PM<sub>2.5</sub> composition, sources and identification of impact areas: From local to long range contributions. *Atmos. Res.* **2017**, *186*, 51–62. [[CrossRef](#)]
13. Avila, A.; Queralt-Mitjans, I.; Alarcón, M. Mineralogical composition of African dust Delivered by red rains over north eastern Spain. *J. Geophys. Res.* **1997**, *102*, 21977–21996. [[CrossRef](#)]
14. Molinaroli, E.; Masiol, M. *Particolato Atmosferico e Ambiente Mediterraneo. Il Caso Delle Polveri Sahariane*; Aracne: Roma, Italy, 2006; p. 224.
15. Jiménez, E.; Linares, C.; Martínez, D.; Díaz, J. Role of Saharan dust in the relationship between particulate matter and short-term daily mortality among the elderly in Madrid (Spain). *Sci. Total Environ.* **2010**, *408*, 5729–5736. [[CrossRef](#)] [[PubMed](#)]
16. Mallone, S.; Stafoggia, M.; Faustini, A.; Gobbi, G.P.; Marconi, A.; Forastiere, F. Saharan dust and associations between particulate matter and daily mortality in Rome, Italy. *Environ. Health Perspect.* **2011**, *119*, 1409–1414. [[CrossRef](#)] [[PubMed](#)]
17. Cadelis, G.; Tourres, R.; Molinie, J. Short-Term Effects of the Particulate Pollutants Contained in Saharan Dust on the Visits of Children to the Emergency Department due to Asthmatic Conditions in Guadeloupe (French Archipelago of the Caribbean). *PLoS ONE* **2014**, *9*, e91136. [[CrossRef](#)] [[PubMed](#)]
18. Middleton, N.; Yiallourous, P.; Kleanthous, S.; Kolokotroni, O.; Schwartz, J.; Dockery, D.W.; Demokritou, P.; Koutrakis, P. A 10-year time-series analysis of respiratory and cardiovascular morbidity in Nicosia, Cyprus: The effect of short-term changes in air pollution and dust storms. *Environ. Health* **2008**, *7*, 1–16. [[CrossRef](#)] [[PubMed](#)]
19. Zhang, X.; Zhao, L.; Tong, D.Q.; Wu, G.; Dan, M.; Teng, B. A Systematic Review of Global Desert Dust and Associated Human Health Effects. *Atmosphere* **2016**, *7*, 158. [[CrossRef](#)]

20. Bennett, C.M.; McKendry, I.G.; Kelly, S.; Denike, K.; Koch, T. Impact of the 1998 Gobi dust event on hospital admissions in the Lower Fraser Valley, British Columbia. *Sci. Total Environ.* **2006**, *366*, 918–925. [[CrossRef](#)] [[PubMed](#)]
21. Schwartz, J.; Norris, G.; Larson, T.; Sheppard, L.; Claiborne, C.; Koenig, J. Episodes of high coarse particle concentrations are not associated with increased mortality. *Environ. Health Perspect.* **1999**, *107*, 339–342. [[CrossRef](#)] [[PubMed](#)]
22. Sandström, T.; Forsberg, B. Desert dust: An unrecognized source of dangerous air pollution? *Epidemiology* **2008**, *19*, 808–809. [[CrossRef](#)] [[PubMed](#)]
23. Pérez, L.L.; Tobias, A.; Querol, X.; Künzli, N.; Pey, J.; Alastuey, A.; Viana, M.; Valero, N.; González-Cabré, M.; Sunyer, J. Coarse particles from Saharan dust and daily mortality. *Epidemiology* **2008**, *19*, 800–807. [[CrossRef](#)] [[PubMed](#)]
24. Chirizzi, D.; Cesari, D.; Guascito, M.R.; Dinoi, A.; Giotta, L.; Donato, A.; Contini, D. Influence of Saharan dust outbreaks and carbon content on oxidative potential of water-soluble fractions of PM<sub>2.5</sub> and PM<sub>10</sub>. *Atmos. Environ.* **2017**, *163*, 1–8. [[CrossRef](#)]
25. Russell, M.; Allen, D.T.; Collins, D.R.; Fraser, M.P. Daily, seasonal, and spatial trends in PM<sub>2.5</sub> mass and composition in southern Texas. *Aerosol Sci. Technol.* **2004**, *38*, 14–26. [[CrossRef](#)]
26. Lianou, M.; Chalbot, M.C.; Kavouras, I.G.; Kotronarou, A.; Karakatsani, A.; Analytis, A.; Katsouyanni, K.; Puustinen, A.; Hameri, K.; Vallius, M.; et al. Temporal variations of atmospheric aerosol in four European urban areas. *Environ. Sci. Pollut. Res.* **2011**, *18*, 1202–1212. [[CrossRef](#)] [[PubMed](#)]
27. Lee, B.K.; Hieu, N.T. Seasonal ion characteristics of fine and coarse particles from an urban residential area in a typical industrial city. *Atmos. Res.* **2013**, *122*, 362–377. [[CrossRef](#)]
28. Mkoma, S.L.; Da Rocha, G.O.; Domingos, J.S.S.; Santos, J.V.S.; Cardoso, M.P.; Da Silva, R.L.; De Andrade, J.B. Atmospheric particle dry deposition of major ions to the South Atlantic coastal area observed at Baía de Todos os Santos, Brazil. *An. Acad. Bras. Cienc.* **2014**, *86*, 37–55. [[CrossRef](#)]
29. Zhang, T.; Cao, J.J.; Tie, X.X.; Shen, Z.X.; Liu, S.X.; Ding, H.; Han, Y.M.; Wang, G.H.; Ho, K.F.; Qiang, J.; et al. Water-soluble ions in atmospheric aerosols measured in Xi’an, China: Seasonal variations and sources. *Atmos. Res.* **2011**, *102*, 110–119. [[CrossRef](#)]
30. Allen, D.T.; Palen, E.J.; Haimov, M.I.; Hering, S.V.; Young, J.R. Fourier transform infrared spectroscopy of aerosol collected in a low pressure impactor (LPI/FTIR): Method development and field calibration. *Aerosol Sci. Technol.* **1994**, *21*, 325–342. [[CrossRef](#)]
31. Maria, S.F.; Russella, L.M.; Turpin, B.J.; Porcja, R.J. FTIR measurements of functional groups and organic mass in aerosol samples over the Caribbean. *Atmos. Environ.* **2002**, *36*, 5185–5196. [[CrossRef](#)]
32. Bruns, E.A.; Perraud, E.; Zelenyuk, A.; Ezell, M.J.; Johnson, S.N.; Yu, Y. Comparison of FTIR and particle mass spectrometry for the measurement of particulate organic nitrates. *Environ. Sci. Technol.* **2010**, *44*, 1056–1061. [[CrossRef](#)]
33. Yu, X.; Song, W.; Yu, Q.; Li, S.; Zhu, M.; Zhang, Y.; Deng, W.; Yang, W.; Huang, Z.; Bi, X.; et al. Fast screening compositions of PM<sub>2.5</sub> by ATR-FTIR: Comparison with results from IC and OC/EC analyzers. *J. Environ. Sci.* **2018**, *71*, 76–88. [[CrossRef](#)]
34. Ghauch, A.; Deveau, P.A.; Jacob, V.; Baussand, P. Use of FTIR spectroscopy coupled with ATR for the determination of atmospheric compounds. *Talanta* **2006**, *68*, 1294–1302. [[CrossRef](#)] [[PubMed](#)]
35. Doyle, W.M. *Principles and Applications of Fourier Transform Infrared (FTIR) Process Analysis*; Technical Note AN-906 Rev. C; Hellma Axiom, Inc.: Plainview, NY, USA, 1992; pp. 1–24.
36. Simonescu, C.M. Application of FTIR Spectroscopy in Environmental Studies. In *Advanced Aspects of Spectroscopy*; Muhammad, A.F., Ed.; InTech: Rijeka, Croatia, 2012; pp. 49–84.
37. Michalski, R. Principles and Applications of Ion Chromatography. In *Application of IC-MS and IC-ICP-MS in Environmental Research*; John Wiley & Sons: Hoboken, NJ, USA, 2016.
38. Rodríguez, S.; Alastuey, A.; Alonso-Pérez, S.; Querol, X.; Cuevas, E.; Abreu-Afonso, J.; Viana, M.; Pérez, N.; Pandolfi, M.; de la Rosa, J. Transport of desert dust mixed with North African industrial pollutants in the subtropical Saharan Air Layer. *Atmos. Chem. Phys.* **2011**, *11*, 6663–6685. [[CrossRef](#)]
39. Pey, J.; Alastuey, A.; Querol, X.; Rodríguez, S. Monitoring of sources and atmospheric processes controlling air quality in an urban Mediterranean environment. *Atmos. Environ.* **2010**, *44*, 4879–4890. [[CrossRef](#)]

40. Putaud, J.P.; Van Dingenen, R.; Alastuey, A.; Bauer, H.; Birmili, W.; Cyrys, J.; Flentje, H.; Fuzzi, S.; Gehrig, R.; Hansson, H.C.; et al. A European aerosol phenomenology e 3: Physical and chemical characteristics of particulate matter from 60 rural, urban, and kerbside sites across Europe. *Atmos. Environ.* **2010**, *44*, 1308–1320. [[CrossRef](#)]
41. Remoundaki, E.; Papayannis, A.; Kassomenos, P.; Mantas, E.; Kokkalis, P.; Tsezos, M. Influence of Saharan Dust Transport Events on PM<sub>2.5</sub> Concentrations and Composition over Athens. *Water Air Soil Pollut.* **2013**, *224*, 1373–1387. [[CrossRef](#)]
42. Amodio, M.; Bruno, P.; Caselli, M.; de Gennaro, G.; Dambruoso, P.R.; Daresta, B.E.; Ielpo, P.; Gungolo, F.; Placentino, C.M.; Paolillo, V.; et al. Chemical characterization of fine particulate matter during peak PM<sub>10</sub> episodes in Apulia (South Italy). *Atmos. Res.* **2008**, *90*, 313–325. [[CrossRef](#)]
43. Cesari, D.; Donato, A.; Conte, M.; Merico, E.; Giangreco, A.; Giangreco, F.; Contini, D. An inter-comparison of PM<sub>2.5</sub> at urban and urban background sites: Chemical characterization and source apportionment. *Atmos. Res.* **2016**, *174–175*, 106–119. [[CrossRef](#)]
44. Vasilatou, V.; Manousakas, M.; Gini, M.; Diapouli, E.; Scoullou, M.; Eleftheriadis, K. Long Term Flux of Saharan Dust to the Aegean Sea around the Attica Region, Greece. *Front. Mar. Sci.* **2017**, *4*, 1–8. [[CrossRef](#)]
45. Nava, S.; Becagli, S.; Calzolari, G.; Chiari, M.; Lucarelli, F.; Prati, P.; Traversi, R.; Udisti, R.; Valli, G.; Vecchi, R. Saharan dust impact in central Italy: An overview on three years elemental data records. *Atmos. Environ.* **2012**, *60*, 444–452. [[CrossRef](#)]
46. Querol, X.; Alastuey, A.; Ruiz, C.R.; Artiñano, B.; Hansson, H.C.; Harrison, R.M.; Buringh, E.; ten Brink, H.M.; Lutz, M.; Bruckmann, P.; et al. Speciation and origin of PM<sub>10</sub> and PM<sub>2.5</sub> in selected European cities. *Atmos. Environ.* **2004**, *38*, 6547–6555. [[CrossRef](#)]
47. Dongarrà, G.; Manno, E.; Varrica, D.; Vultaggio, M.; Lombardo, M. Study on ambient concentrations of PM<sub>10</sub>, PM<sub>10-2.5</sub>, PM<sub>2.5</sub> and gaseous pollutants. Trace elements and chemical speciation of atmospheric particulates. *Atmos. Environ.* **2010**, *44*, 5244–5257. [[CrossRef](#)]
48. Pastuszka, J.S.; Rogula-Kozłowska, W.; Zajusz-Zubek, E. Characterization of PM<sub>10</sub> and PM<sub>2.5</sub> and associated heavy metals at the crossroads and urban background site in Zabrze, Upper Silesia, Poland, during the smog episodes. *Environ. Monit. Assess.* **2010**, *168*, 613–627. [[CrossRef](#)] [[PubMed](#)]
49. Ferm, M.; Sjöberg, K. Concentrations and emission factors for PM<sub>2.5</sub> and PM<sub>10</sub> from road traffic in Sweden. *Atmos. Environ.* **2015**, *119*, 211–219. [[CrossRef](#)]
50. Kouyoumdjian, H.; Saliba, N.A. Mass concentration and ion composition of coarse and fine particles in an urban area in Beirut: Effect of calcium carbonate on the absorption of nitric and sulfuric acids and the depletion of chloride. *Atmos. Chem. Phys.* **2006**, *6*, 1865–1877. [[CrossRef](#)]
51. Hug, S. In situ Fourier Transform infrared measurements of sulfate adsorption on hematite in aqueous solutions. *J. Colloid Interface Sci.* **1997**, *188*, 415–422. [[CrossRef](#)]
52. Peak, D.; Ford, R.G.; Sparks, D.L. An in situ ATR-FTIR investigation of sulfate bonding mechanisms on Goethite. *J. Colloid Interface Sci.* **1999**, *218*, 289–299. [[CrossRef](#)] [[PubMed](#)]
53. Shaka, H.; Saliba, N. Concentration measurements and chemical composition of PM<sub>10-2.5</sub> and PM<sub>2.5</sub> at a coastal site in Beirut, Lebanon. *Atmos. Environ.* **2004**, *38*, 523–531. [[CrossRef](#)]
54. Rodriguez-Navarro, C.; Sebastian, E. Role of particulate matter from vehicle exhaust on porous building stones (limestone) sulfation. *Sci. Total Environ.* **1996**, *187*, 79–91. [[CrossRef](#)]
55. Varrica, D.; Dongarrà, G.; Sabatino, G.; Monna, F. Inorganic geochemistry of roadway dust from the metropolitan area of Palermo (Italy). *Environ. Geol.* **2003**, *44*, 222–230. [[CrossRef](#)]
56. Montana, G.; Randazzo, L.; Oddo, I.A.; Valenza, M. The growth of “black crusts” on calcareous building stones in Palermo (Sicily): A first appraisal of anthropogenic and natural sulphur sources. *Environ. Geol.* **2008**, *56*, 367–380. [[CrossRef](#)]
57. Rahier, H.; Wullaert, B.; Van Mele, B. Influence of the Degree of Dehydroxylation of Kaolinite on the Properties of Aluminosilicate Glasses. *J. Therm. Anal. Calorim.* **2000**, *62*, 417–427. [[CrossRef](#)]
58. Chou, C.C.K.; Huang, S.H.; Chen, T.K.; Lin, C.Y.; Wang, L.C. Size-segregated characterization of atmospheric aerosols in Taipei during Asian outflow episodes. *Atmos. Res.* **2005**, *75*, 89–109. [[CrossRef](#)]
59. Coury, C.; Dillner, A.M. A method to quantify organic functional groups and inorganic compounds in ambient aerosols using attenuated total reflectance FTIR spectroscopy and multivariate chemometric techniques. *Atmos. Environ.* **2008**, *42*, 5923–5932. [[CrossRef](#)]

60. Reff, A.; Turpin, B.J.; Offenberg, J.H.; Weisel, C.P.; Zhang, J.; Morandi, M.; Stock, T.; Colome, S.; Winer, A. A functional group characterization of organic PM 2.5 exposure: Results from the RIOPA study. *Atmos. Environ.* **2007**, *41*, 4585–4598. [[CrossRef](#)]
61. Coury, C.; Dillner, A.M. ATR-FTIR characterization of organic functional groups and inorganic ions in ambient aerosols at a rural site. *Atmos. Environ.* **2009**, *43*, 940–948. [[CrossRef](#)]
62. Madejová, J.; Komadel, P. Baseline Studies of the Clay Minerals Society Source Clays: Infrared Methods. *Clays Clay Miner.* **2001**, *49*, 410–432. [[CrossRef](#)]
63. Davarcioglu, B. Spectral characterization of non-clay minerals found in the clays Central Anatolian-Turkey. *Int. J. Phys. Sci.* **2011**, *6*, 511–522.
64. Wilson, M.J. *A Handbook of Determinative Methods in Clay Mineralogy*; Blackie-Son Ltd.: London, UK, 1987; p. 308.
65. Suárez, M.; García-Romero, E. FTIR spectroscopic study of palygorskite: Influence of the composition of the octahedral sheet. *Appl. Clay Sci.* **2006**, *31*, 154–163. [[CrossRef](#)]
66. Anton, O.; Rouxhet, P.G. Note on the intercalation of kaolinite, dickite, and halloysite by dimethylsulfoxide. *Clays Clay Miner.* **1977**, *25*, 259–263. [[CrossRef](#)]
67. Madejová, J. FTIR techniques in clay mineral studies. *Vib. Spectrosc.* **2003**, *31*, 1–10. [[CrossRef](#)]
68. Farmer, V.C. Transverse and longitudinal crystal modes associated with OH stretching vibrations in single crystals of kaolinite and dickite. *Spectrochim. Acta* **2000**, *56*, 927–930. [[CrossRef](#)]
69. Cheng, Z.L.; Lam, K.S.; Chan, L.Y.; Wang, T.; Cheng, K.K. Chemical characteristics of aerosols at coastal station in Hong Kong. I. Seasonal variation of major ions, halogens and mineral dusts between 1995 and 1996. *Atmos. Environ.* **2000**, *34*, 2771–2783. [[CrossRef](#)]
70. Kong, L.; Yang, Y.; Zhang, S.; Zhao, X.; Du, H.; Fu, H.; Zhang, S.; Cheng, T.; Yang, X.; Chen, J.; et al. Observations of linear dependence between sulfate and nitrate in atmospheric particles. *J. Geophys. Res. Atmos.* **2013**, *119*, 341–361. [[CrossRef](#)]
71. Squizzato, S.; Masiol, M.; Brunelli, A.; Pistollato, S.; Tarabotti, E.; Rampazzo, G.; Pavoni, B. Factors determining the formation of secondary inorganic aerosol: A case study in the Po Valley (Italy). *Atmos. Chem. Phys.* **2013**, *13*, 1927–1939. [[CrossRef](#)]
72. Baek, B.H.; Aneja, V.P.; Tong, Q. Chemical coupling between ammonia, acid gases, and fine particles. *Environ. Pollut.* **2004**, *129*, 89–98. [[CrossRef](#)] [[PubMed](#)]
73. Huang, X.; Qiu, R.; Chan, C.K.; Kant, P.R. Evidence of high PM<sub>2.5</sub> strong acidity in ammonia-rich atmosphere of Guangzhou, China: Transition in pathways of ambient ammonia to form aerosol ammonium at  $[\text{NH}_4^+]/[\text{SO}_4^{2-}] = 1.5$ . *Environ. Res.* **2011**, *99*, 488–495. [[CrossRef](#)]
74. Pio, C.A.; Cerqueira, M.A.; Castro, L.M.; Salgueiro, M.L. Sulphur and nitrogen compounds in variable marine/continental air masses at the South-west European coast. *Atmos. Environ.* **1996**, *30*, 3115–3127. [[CrossRef](#)]

